

AMMONIA GAS SENSING PROPERTIES AT LOW TEMPERATURE OF GRAPHENE OXIDE/TUNGSTEN OXIDE NANOBLOCKS NANOCOMPOSITES

Nguyen Cong Tu^{1,*}, Nguyen Anh Kiet¹, Phung Nhat Minh¹, Ngo Xuan Dinh²,
Le Anh Tuan², Luu Thi Lan Anh¹, Do Duc Tho¹, Nguyen Huu Lam¹

¹*School of Engineering Physics, Hanoi University of Science and Technology,
No 1, Dai Co Viet street, Ha Noi, Viet Nam*

²*Phenikaa University Nano Institute, Phenikaa University, Yen Nghia ward,
Ha Dong district, Ha Noi, Viet Nam*

*Email: tu.nguyencong@hust.edu.vn

Received: 17 December 2019; Accepted for publication: 25 March 2020

Abstract. Nanocomposites of graphene oxide (GO) and tungsten oxide (WO₃) nanobricks were synthesized by co-dispersing graphene oxide and tungsten oxide nanobricks in bi-distilled water with different weight ratios (0.1, 0.3 and 0.5 wt.% of graphene oxide). The ammonia gas sensing properties of nanocomposites were studied at low temperatures (50, 100 and 150 °C) with the static gas-testing system. The co-appearance and the strong interaction between graphene oxide and tungsten oxide in the nanocomposite were confirmed by Raman scattering analysis. The content of GO in nanocomposite strongly affects the resistance of nanocomposite-based sensors. When the working temperature increase from 50 °C to 150 °C, the response of sensors switches from the *p*-type (at 50 °C) to *n*-type (at 150 °C) behavior. At 150 °C, the nanocomposite-based sensors show the most stable ammonia gas sensing characteristics. The working resistance of the pristine WO₃ sensor reduced from 1.35 MΩ to 90, 72 and 27 kΩ when compositing with 0.1, 0.3 and 0.5 wt.% GO at 150 °C, respectively. The 0.5 wt.% GO/WO₃ -based sensor shows low response but low working resistance, shorter response and recovery times (20 s and 280 s, respectively) which is promising for low power-consumption gas sensors.

Keywords: GO, tungsten oxide nanobricks, nanocomposite, low-resistance gas sensor.

Classification numbers: 2.4.2, 2.4.4, 2.9.4.

1. INTRODUCTION

Since the first fabrication in 2007 by Geim and Novoselov, graphene (Gr) become a nascent star in material science and attracted a lot of attention due to its outstanding properties [1]. But due to the edge effect, the low dispersion in an aquatic environment and the limit of technology, the application of Gr is limited which results in the decrement of the interest on the pristine Gr in the middle of 2010s [2]. Recently, the interest on Gr-based materials is once more blooming due to the appearance of graphene's derivatives (graphene oxide - GO, reduced graphene oxide - rGO) which having higher dispersibility in aquatic environment and the

appearance of nanocomposite materials of Gr-based materials with noble metals [3], metal oxide semiconductors [4 - 8]. In these brand-new Gr-based materials, the most studied family is composite or hybrid material of Gr or its derivatives with metal oxide semiconductors to enhance photocatalytic activity [8], possibility in energy storage [5], toxic gas sensing characteristics [9], and effectivity in pollutant removal [7]. The aim of using Gr and its derivatives in these composition/hybridizations are to enhance the surface area and the lifetime of the carriers in photocatalyst application [10]; to create heterojunction and reduce working resistance in gas sensor applications [11, 12].

In gas sensor researches, especially hazardous gas sensors like ammonia gas sensors, the two most important tasks are lowering the working temperature and reducing working resistance [13, 14]. Lowering the working temperature not only lowers consuming power providing for the heating section but also avoids the grain coalescence of nanostructures happening in long-term operations at high temperatures (at > 200 °C) [15]. The grain coalescence could cause the change in crystal structure even after processing at a high temperature which might cause the change of gas sensing characteristic – degradation of the gas sensor. Reducing the resistance of sensors not only helps increase measurement accuracy by increasing the signal to noise ratio but also helps simplify the design of the sensor by removing the signal amplification module [14, 16 - 18]. To reach two goals, one of the most preferable routes is compositing, hybridizing or decorating Gr and its derivatives with traditional metal oxide semiconductors in gas sensor applications such as SnO₂, ZnO, WO₃, etc. [9]. Among these metal oxide semiconductors, tungsten oxide (WO₃) is a widely studied material due to its unique physicochemical properties such as stability in both acid and base environments [19, 20]. Recently, Chu *et al.* studied the ammonia (NH₃) gas sensing characteristic at high temperature (> 200 °C) of rGO/WO₃ nanowire nanocomposite prepared via hydrothermal process [21]; Salam *et al.* enhanced the NH₃ gas sensing activity at 200 °C of hexagonal WO₃ nanorods by interspersing GO in WO₃ nanorods via hydrothermal method [22]. Jeevitha *et al.* prepared porous rGO/WO₃ nanocomposites for enhancing the detection of NH₃ at room temperature [23].

In this work, the authors composite GO with WO₃ nanobricks (NBs) to reduce the resistance of gas sensors and study the effect of GO content on the NH₃ gas-sensing characteristic of composite-based sensors. Stable monoclinic WO₃ NBs were synthesized by an one-step hydrothermal method. GO was synthesized following the Hummers method [24]. WO₃ NBs and GO were composited with different contents via co-dispersing in bi-distilled water. The NH₃ gas-sensing properties of nanocomposite materials were investigated at low temperatures (50, 100 and 150 °C). In this study, Raman scattering is used to investigate the interaction between WO₃ and GO in nanocomposite materials. The role of WO₃ NBs in the nanocomposite is also discussed.

2. EXPERIMENTAL

2.1. Samples preparation

Tungsten oxide NBs were synthesized using the hydrothermal method by dissolving 8.25 g of Na₂WO₄·2H₂O into 25 mL of bi-distilled water, adding dropwise 45 ml of HCl (37 wt. %) into the above solution. The prepared solution was placed into a Teflon-lined stainless-steel autoclave, and then the hydrothermal process was performed at 180 °C for 48 h. The obtained slurry was cleaned and filtered with bi-distilled water using 15- μ pore-size filter paper. The cleaned slurry was dried

in ambient air and then ground to obtain powders. The detail of the preparation process could be found in our previous work [25].

GO was prepared via Hummers method [24] as follows: 0.5 g of graphite flake, 0.25 g of NaNO_3 were dissolved into 40 ml H_2SO_4 (98 %), the obtained solution was stirred vigorously at 0 °C for 2 h; adding 2 g KMnO_4 and stirring for 48 h; adding 25 ml distilled water into obtained solution and stirring at 95 °C for 1 h, then cooling down to room temperature and adding 25 ml distilled water and 3 ml H_2O_2 to obtain multilayer graphite oxide; graphite oxide was then cleaned and filtered three times by HCl (3M), centrifugated with speed of 14000 revs/min to obtain graphene oxide (GO). GO was then dispersed in distilled water to get GO suspension of 100 ppm concentration.

In order to prepare nanocomposite-based sensors, different suspensions of nanocomposite (WO_3 and GO) having different GO content were prepared via following steps: first, mixing 1, 3 and 5 ml of 100-ppm GO suspension with 4, 2 and 0 ml bi-distilled water to prepare 5-ml GO suspensions which have 0.0001, 0.0003 and 0.0005 g GO, respectively; then, dispersing 0.0999, 0.0997 and 0.0995 g WO_3 powder into 5-ml GO suspensions having 0.0001, 0.0003 and 0.0005 g GO, respectively, to prepare 5-ml nanocomposite suspensions in which all the total amount of nanocomposite (WO_3 +GO) is 0.1000 g. The obtained nanocomposite suspensions were kept in the ultrasonic bath for 10 mins to make the uniform dispersion. Then, the nanocomposite suspensions were deposited on comb-type Pt electrodes (patterned on SiO_2/Si substrates) by the drop-coating method. The drop-coated electrodes were annealed at 200 °C for 3 h to remove the water solvent and stabilize the sensors. The pristine WO_3 -based sensor was prepared via a similar process but using a suspension of 0.1 g WO_3 powder in 5 ml water for comparison (The components of nanocomposite and WO_3 suspensions are listed in Table S1). After annealing, the sensors were used for the NH_3 gas-sensing study.

2.2. Analysis

The high magnification field-emission scanning electron microscopy (FESEM, HITACHI S4800) was used to study the morphology of tungsten oxide nanostructure. Low magnification SEM images and mapping energy-dispersive X-ray spectroscopy (EDS) images of samples were captured by Tabletop Microscope HITACHI TM4000Plus. The crystalline properties of the samples were characterized by using X'pert Pro (PANalytical) MPD with $\text{CuK-}\alpha 1$ radiation ($\lambda = 1.54065 \text{ \AA}$) at a scanning rate of $0.03^\circ/2 \text{ s}$ in the 2θ range of 20° - 80° . Crystal analysis was performed by HighScore Plus software using the ICDD database. The Fourier transform infrared spectrum (FTIR) of GO was acquired by using Fourier transform infrared spectrophotometer IRAffinity-1S, SHIMADZU. The micro Raman spectra were observed by Renishaw InVia Raman Microscope using a 633 nm laser. The NH_3 gas-sensing properties of the sensors were analyzed by placing NH_3 vapor into the closed chamber (NH_3 is equivalent to 76 ppm measured by a Canadian BW gas alert device) and measuring the resistance of the sensors using a Keithley 6487 picometre/voltage source at elevated temperatures (50, 100 and 150 °C).

3. RESULTS AND DISCUSSIONS

3.1 Characterization of WO_3 and GO

Figure 1a presents the FESEM image of as-grown tungsten oxide nanostructure. The morphology of tungsten oxide nanobricks appears uniformly with the approximate medium

dimensions of 60 nm × 60 nm × 100 nm. FESEM image also implies that tungsten oxide nanobricks were well separated and nanobricks had sharp corners. The sharp and strong peaks in the XRD pattern of tungsten oxide NBs (Fig. 1b) implied the high crystallinity and uniformity of the tungsten oxide NBs. XRD analysis using HighScore Plus software showed that tungsten oxide NBs had a stable crystal structure [19, 25]– monoclinic WO₃ (ICDD Card No.01-071-2141) (Fig. 1b), and no peak of any other phases or impurities appeared in the XRD pattern. In this work, we used the as-grown monoclinic WO₃ nanobricks to composite directly with GO without any further annealing treatment.

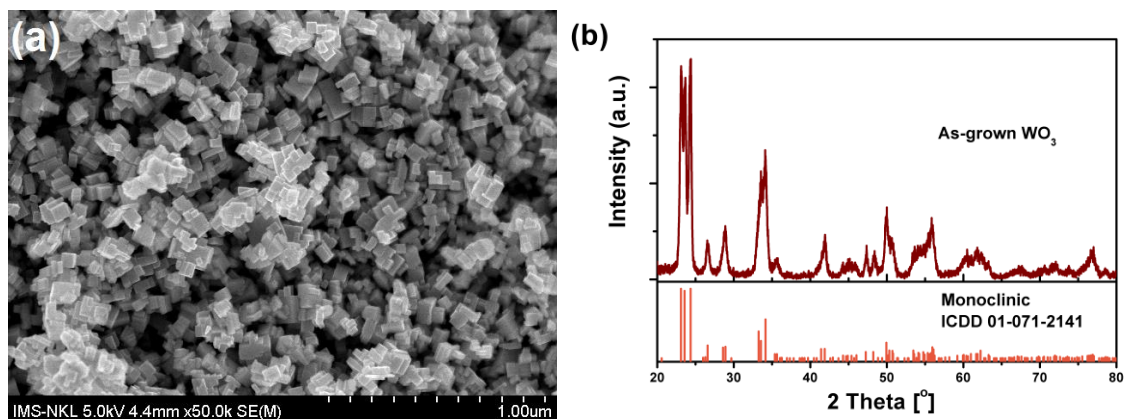


Figure 1. (a) FESEM image of as-grown WO₃ nanobricks and (b) XRD pattern of as-grown WO₃ in comparison with the standard pattern of monoclinic WO₃ (ICDD card No 01-071-2141).

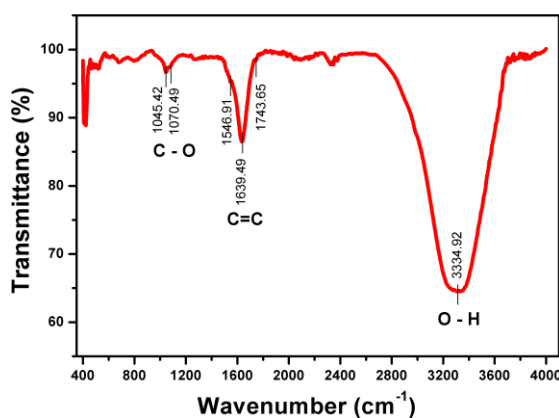


Figure 2. FTIR spectrum of GO suspension.

To verify the formation of GO in the obtained suspension, the FTIR spectrum of obtained suspension was examined. Figure 2 presents the FTIR spectrum of GO. In the FTIR spectrum of GO, the characteristic peaks of GO are observed. The strong and broad peak at 3334.92 cm⁻¹ attributed to the O-H stretch of H₂O molecules absorbed in GO. The peaks at 1743.65 and 1070.49 cm⁻¹ originate from the C=O and C-O bonds, respectively. The appearance of these peaks confirms the presence of oxide function groups after the oxidation process [24, 26] which also confirms the successful preparation of GO.

3.2. GO/WO₃ nanocomposite

Due to the strong energy of the electron beam in FESEM, the electron beam can easily penetrate through the several-layered GO which causes difficulty in observing the appearance of GO on the surface of GO/WO₃ using FESEM. To examine the appearance of GO on the surface of GO/WO₃ composite, we use low magnification SEM. Fig. 3a presents the low magnification SEM image of sample 0.5 % GO/WO₃ in which the opaque on the surface of the composite is assigned to the GO. The distribution of GO in the nanocomposite samples is studied via analyzing the distribution of carbon (C) element in mapping EDS images of the sample 0.5 wt.% (Fig. S1). The results show that the carbon (C) element is homogeneously distributed in the EDS image (Fig. S1b) which implies the homogeneous distribution of GO in the nanocomposite.

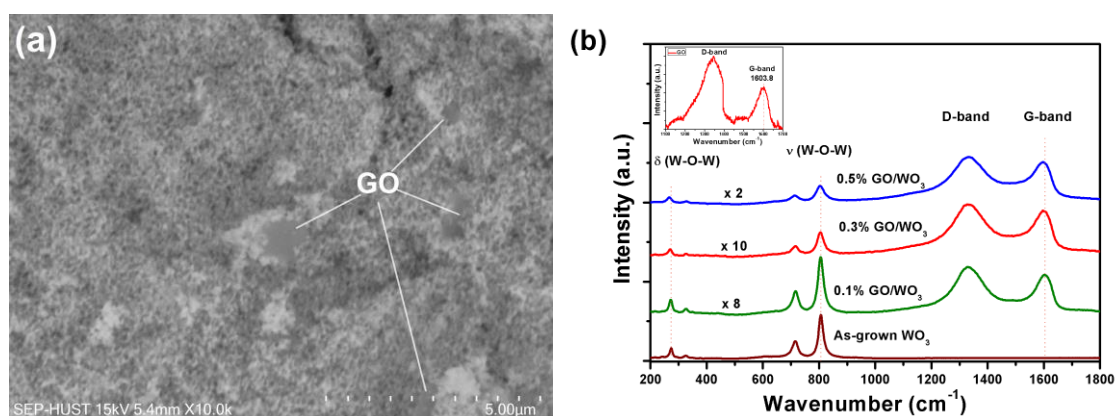


Figure 3. (a) Low magnification SEM image of sample 0.5 % GO@WO₃ and (b) Raman spectra of all samples. The inset is the Raman spectrum of as-prepared GO.

The co-appearance of WO₃ and GO in nanocomposite is also confirmed with Raman scattering analysis. Fig. 3b manifests the Raman spectra of both pristine and composite samples. In the Raman spectra of hybrid samples, the typical peaks of monoclinic WO₃ at ~ 270, and 805 cm⁻¹ and typical D- and G-bands of GO at ~1330 and 1600 cm⁻¹ are observed [27]. The position of the characteristic peaks of both WO₃ and GO are listed in Table 1. The co-appearance of these typical peaks and bands strongly confirms the co-existence of WO₃ and GO in composite samples. We also observe the increase of intensity ratio of G-band and the peak at ~ 805 cm⁻¹ with the increasing GO content. In the Raman spectra, the shift of typical peaks and bands of both WO₃ and GO are perceived. The characteristic peak of WO₃ at 270 cm⁻¹ originates from the bending vibration $\delta(\text{O-W-O})$ of bridging oxygen [28]. The characteristic peak at ~805 cm⁻¹ originates from the stretching vibration $\nu(\text{O-W-O})$ of W-O binding in monoclinic WO₃ [29]. Both typical peaks of $\delta(\text{O-W-O})$ and $\nu(\text{O-W-O})$ are shifted to the lower wavenumber in the hybrid samples (note in Fig. 2) which implies the interaction between GO and WO₃. The shift is further in the higher GO-content hybrid samples which means the stronger interaction between GO and WO₃ nanobricks. The left shift of G-band in composite samples (from 1603.8 in GO to 1602.5, 1599.1 and 1597.1 cm⁻¹ in composite samples) also gives a proof of the interaction between GO and WO₃ implying the charge transfer between GO and WO₃ [14, 30]. The widening of the peak at ~ 805 cm⁻¹ is another convincing proof of the robust hybridization of GO in WO₃ platform materials [31]. These proofs confirm the strong interaction between GO and WO₃ in

nanocomposite material which indicates the hybridization instead of physical mixing between GO and WO₃.

The intensity ration between D-band and G-band is another important parameter in evaluating the carbon-based composite materials. Results in Table 1 show that the I_D/I_G ratio decrease from 1.74 in pristine GO to 1.19, 1.13 and 1.12 in 0.1, 0.3 and 0.5 % GO@WO₃, respectively. The reason for this decrease might be due to the stacking effect, i.e. the natural trend of graphene-based materials in solution [32 - 34]. During the annealing process, the stacking phenomenon happens strongly which results in the thicker GO layer, lower surface area to volume ratio and lower I_D/I_G ratio in comparison with pristine GO. The stacking effect is stronger in a higher GO-content sample which causes the decrement of I_D/I_G ratio from 1.19 to 1.13 and 1.12 when the GO content increases from 0.1 to 0.3 and 0.5 %, respectively. Due to this stacking effect, in our work, the GO content is limited at 0.5 %.

Table 1. Position of the characteristic Raman peaks of WO₃ and GO in pristine and hybrid samples.

Peak	WO ₃	0.1%GO @WO ₃	0.3%GO @WO ₃	0.5%GO @WO ₃	GO
$\nu(\text{O-W-O})$	805.9	805.4	804.6	803.9	-
$\delta(\text{O-W-O})$	273.9	272.1	269.9	265.9	-
G-band	-	1602.5	1599.1	1597.1	1603.8
I _D /I _G	-	1.19	1.13	1.12	1.74

3.3. Gas sensor properties

Figure 4a-c shows the response of the nanocomposite-based sensor with 76 ppm NH₃ at low temperatures (50, 100 and 150 °C). The WO₃ NB-based sensor shows a good response to NH₃ [14] but due to large resistance (1.35 MΩ at 150 °C), WO₃ NB-based sensor was not further studied in this research. Fig. 4d presents the response of nanocomposite-based sensors at different temperatures. The response of the sensor was defined by the ratio $(R_{gas} - R_{air})/R_{air}$, in which R_{air} is the sensor's resistance in ambient air, and R_{gas} is the sensor's resistance in NH₃ gas environment. Graphene and its derivatives are counted as a p-type semiconductor which increases the resistance (positive response) when exposing to NH₃ [12]. WO₃ is naturally counted as an n-type semiconductor which will decrease the resistance (negative response) when exposing to NH₃ [35]. But all nanocomposite-based sensors show a p-type response to NH₃ at 50, 100 °C (positive response) then change to n-type behavior at 150 °C (negative response). At 50 °C, all sensors manifest the highest but unstable response and large baseline shift. When working temperature increases from 50 to 100 °C, the absolute response of nanocomposite-based sensors decreases: sample 0.1 wt.% GO@WO₃ decreases from 106.4 to 6.5 %; sample 0.3 wt.% GO@WO₃ decreases from 15.8 to 2.4 %; sample 0.5 wt.% GO@WO₃ decreases from 21.0 to 11.4 %. When working temperature reaches to 150 °C, the absolute value of response increases again and the behavior change from p-type to n-type: the absolute value of response of sample 0.1 wt.% GO@WO₃ increases to 30.0 %; of sample 0.3 wt.% GO@WO₃ increases to 11.0 %; of sample 0.5 wt.% GO@WO₃ increases to 13 %. At 150 °C, nanocomposite-based sensors show the most stable gas sensing characteristics: having a small baseline shift and/or clear getting to a stable value of the response.

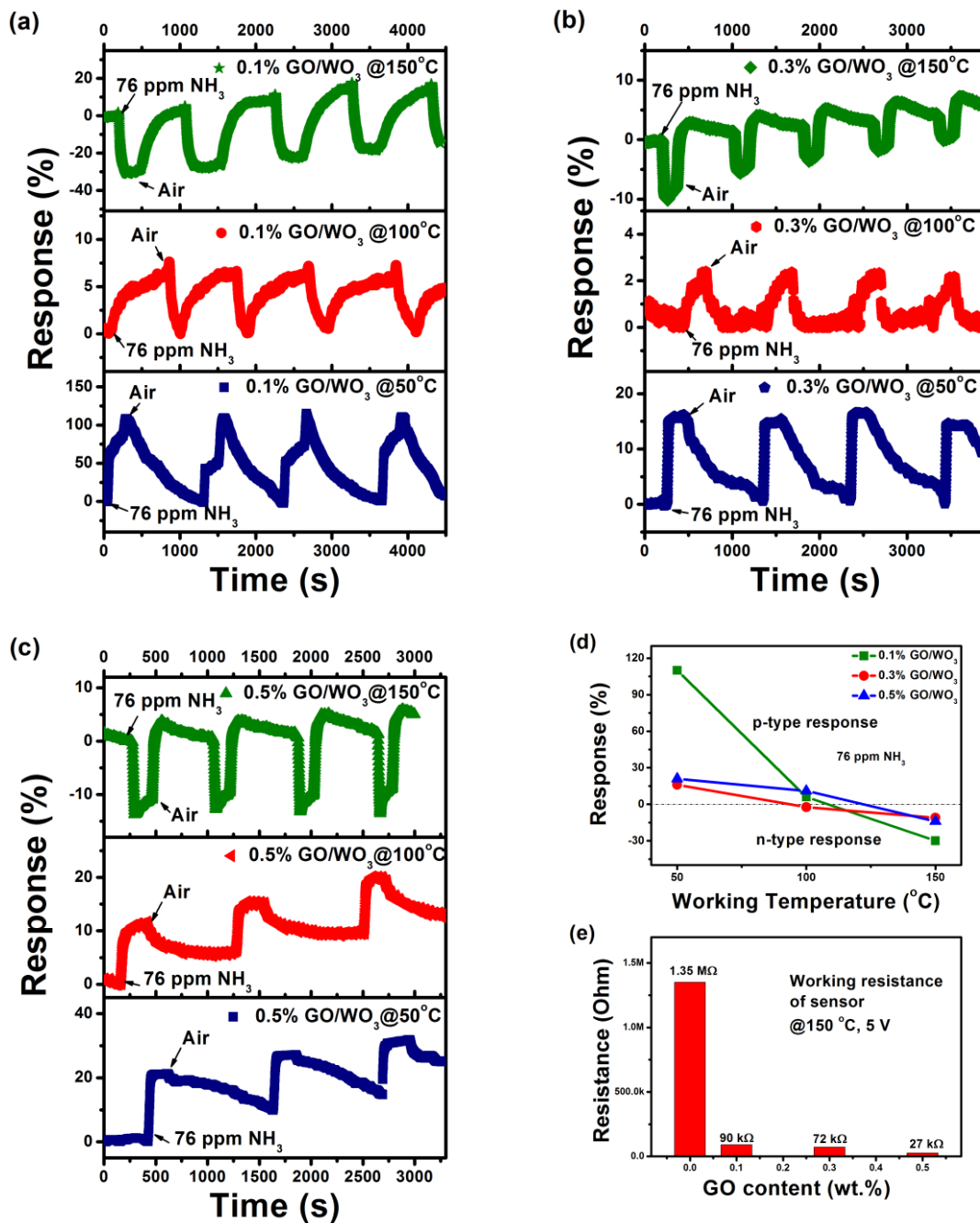


Figure 4. The response revolution of (a) 0.1 wt.% GO/WO₃, (b) 0.3 wt.% GO/WO₃, (c) 0.5 wt.% GO/WO₃ composite-based sensors with 76 ppm NH₃ at 50, 100 and 150 °C; (d) the response of sensors with 76 ppm NH₃ at different temperatures and (e) the working resistance of sensors at 150 °C under 5-V bias voltage.

The change from n-type to p-type behavior of the composite-based sensor when temperature increases is assigned to the change of behavior of WO₃ with temperature. The switch between n-type and p-type behaviors is common in semiconductor metal oxide gas sensor

which might be attributed to one of four reasons [35]: (i) the change of prominent charge carrier (donor or acceptor) density in bulk; (ii) the change in temperature reactions (the reaction between materials and gas is activated by heat); (iii) the changes in the prevailing oxygen partial pressure; and (iv) the appearance of foreign gas in an air ambient when the bulk donor density and acceptor density of an oxide close to the minimum value. In this work, the reason for the switching behavior of WO_3 is none of the above four reasons but the inversion effect caused by the strong adsorption of oxygen and water molecules on the WO_3 surface [14, 36]. The mechanism of the inversion effect at low temperature is presented in Fig. 5. H_2O and O_2 absorbed on the WO_3 surface take natural electrons from the WO_3 surface to create $\cdot\text{OH}$, O_2^- agents which then accumulate to form a rich negative-carrier layer around WO_3 surface. This layer then creates a positive layer on the WO_3 surface (inversion layer) through the induction effect. In the inversion effect, H_2O keeps the vital role which will be lessened or eliminated in higher temperature (100 and 150 °C). At 50 °C, the inversion effect strongly appears resulting the strong p-type behavior. At 100 °C, the absorption of H_2O on WO_3 decreases which causes the smaller p-type response. At 150 °C, the inversion effect is eliminated due to no H_2O molecule is absorbed on the WO_3 surface and WO_3 shows the natural n-type characteristic. The change of nanocomposite-based behavior with temperature due to the change of WO_3 behavior causes also implies the dominant role of WO_3 in gas sensing activity of nanocomposite-based sensors. Due to this inversion effect, the NH_3 gas-sensing characteristic of nanocomposite and pristine WO_3 are unstable at 50 and 100 °C. This is the reason we choose the working temperature is 150 °C for further study.

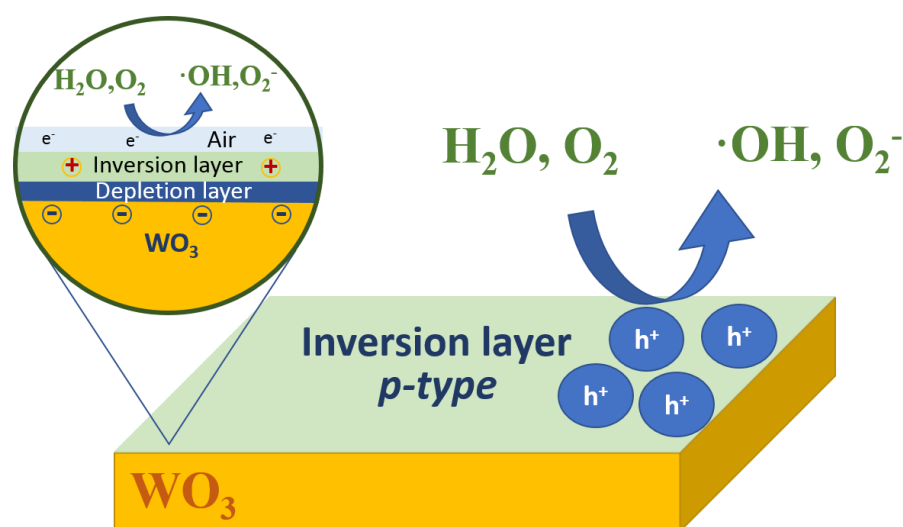


Figure 5. The mechanism of inversion effect on the surface of WO_3 at low temperature.

At 150 °C, the working resistance of composite sensor decrease with the increase of GO content in composite materials. The resistance of the sensor decreases from 1.35 M Ω to 90, 72 and 27 k Ω when the GO content increase from 0 to 0.1, 0.3 and 0.5 wt.%, respectively (Fig. 4e). These values are suitable for low power consumption gas sensors [16]. In three nanocomposite-based sensors, 0.1 wt.% GO/ WO_3 sensor shows the highest response (-30 %) but the baseline is shifted to a higher value, and it takes the longest time to respond to NH_3 (80 s) and to recover (270 s) (Fig. S2a). The 0.3 wt.% GO/ WO_3 sensor has the lowest response (-11 %), shifting

baseline, longer recovery time (300 s) but the much shorter response time (26 s) than 0.1 wt.% (Fig. S2.b). The 0.5 wt.% GO/WO₃ sensor show low response (-13 %) but small baseline shift, shortest response and recovery times, i.e. 20 and 250 s, respectively (Fig. S2.c). Clearly, the 0.5 wt.% GO/WO₃ sensor shows the best characteristic in NH₃ gas-sensing properties among the nanocomposite-based sensors (Fig. 6). The 0.5 wt.% GO/WO₃ nanocomposite-based sensor has a lower response but lower working resistance, smaller baseline shift, and shorter response and recovery times. These characteristics imply that 0.5 wt.% GO/WO₃ is a good candidate for low power-consumption gas sensor applications [14, 16, 37]. The results obtained with sample 0.5 wt.% GO/WO₃ is similar to the result obtained by Jeevitha *et al.* [23] and is higher than the results obtained by Salama *et al.* [22]. Jeevitha *et al.* obtains the highest response of 13 % at room temperature with 80 ppm NH₃ but higher resistance of ~ 1.25 MΩ [23]. Salama *et al.* obtain only an 8 % response with 70 ppm NH₃ at 200 °C [22].

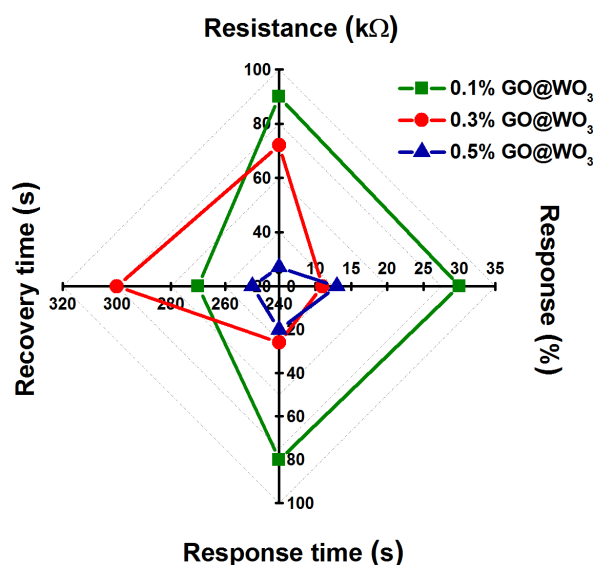


Figure 6. The gas sensing characteristics of nanocomposite-based sensors at 150 °C temperature.

4. CONCLUSION

Nanocomposites of GO and WO₃ NBs with different GO contents (0.1, 0.3 and 0.5 %wt.) were synthesized by co-dispersing GO and WO₃ in bi-distilled water. The shift of characteristic peaks in the Raman spectra of composite materials manifests the strong interaction between WO₃ NBs and GO and confirms that the composite material is not only a physical mixture of WO₃ and GO. The nanocomposite-based sensors show good responses to NH₃ but the behavior switches when working temperature increase - change from the p-type response at 50 and 100 °C to the n-type response at 150 °C. The switching behavior is assigned to the strong inversion effect appearing on the WO₃ surface at 50 and 100 °C due to the strong adsorption of H₂O on the WO₃ surface. The switch also implies the dominant role of WO₃ in the nanocomposite-based sensor. At 150 °C, all sensors show the stable gas sensing characteristic: having a small baseline shift, independence from inversion effect caused by adsorption of H₂O. The working resistance of the nanocomposite-based sensor decreases in comparison with the pure WO₃ sensor. At 150 °C, the working resistance under 5-V bias reduces from 1.35 MΩ in pure WO₃ sensor to 90, 72 and 27 kΩ in 0.1, 0.3 and 0.5 wt.% GO/WO₃ nanocomposite-based sensor. All composite sensors show n-

type responses to NH₃ which implies the predominant role of WO₃ in the composite-based sensor. Among three samples, the 0.5 wt.% GO/WO₃ sensor shows low response (-13 % to 76 ppm NH₃) but has good gas sensing characteristics such as shortest response time (20 s) and lowest working resistance (27 kΩ). These characteristics imply that 0.5 wt.% GO/WO₃ composite material is a good candidate for a low power-consumption NH₃ gas sensor. The results suggest a simple method to fabricate GO/WO₃ composite material for many applications such as gas sensors, electrochromic, and photocatalytic applications.

Acknowledgements. This research is funded by Vietnam National Foundation for Science and Technology Development (NAFOSTED) under Grant number 103.02-2019.13.

REFERENCES

1. Geim A. K. and Novoselov K. S. - The rise of graphene, *Nat. Mater.* **6** (2007) 183-191.
2. Chen D., Tang L., and Li J. - Graphene-based materials in electrochemistry, *Chem. Soc. Rev.* **39** (2010) 3157-3180.
3. Tan C., Huang X., and Zhang H.- Synthesis and applications of graphene-based noble metal nanostructures, *Mater. Today* **16** (2013) 29-36.
4. Majeed A., Ullah W., Waheed A., Nasreen F., and Sharif A. - Graphene-metal oxides/hydroxide nanocomposite materials: Fabrication advancements and supercapacitive performance, *J. Alloys Compd.* **671** (2016) 1-10.
5. Hau Low W., Sim Khiew P., Shee Lim S., Wee Siong C., and Raphael Ezeigwe E. - Recent development of mixed transition metal oxide and graphene/mixed transition metal oxide based hybrid nanostructures for advanced supercapacitors, *J. Alloys Compd.* **775** (2019) 1324-1356.
6. Huang Z. F., Song J., Pan L., Zhang X., Wang L., and Zou J. J.- Tungsten oxides for photocatalysis, electrochemistry, and phototherapy, *Adv. Mater.* **27** (2015) 5309-5327.
7. Khan M., Tahir M. N., Adil S. F., Khan H. U., Siddiqui M. R. H., Al-warthan A. A., and Tremel W. - Graphene based metal and metal oxide nanocomposites: synthesis, properties and their applications, *J. Mater. Chem. A* **3** (2015) 18753-18808.
8. El-shafai N. M., El-khouly M. E., El-kemary M., Ramadan M. S., and Masoud M. S. - Graphene oxide–metal oxide nanocomposites: fabrication, characterization and removal of cationic rhodamine B dye, *RSC Adv.* **8** (2018) 13323-13332.
9. Gupta S., Chatterjee S., Ray A. K., and Chakraborty A. K. - Graphene – metal oxide nanohybrids for toxic gas sensor: A review, *Sensors Actuators B. Chem.* **221** (2015) 1170-1181.
10. Hossain S., Chu W., Sunyong C., Ahn S., and Chun D. - Photocatalytic performance of few-layer graphene/WO₃ thin films prepared by a nano-particle deposition system, *Mater. Chem. Phys.* **226** (2019) 141-150.
11. Chang X., Zhou Q., Sun S., Shao C., and Lei Y. - Graphene-tungsten oxide nanocomposites with highly enhanced gas- sensing performance, *J. Alloys Compd.* **705** (2017) 659-667.
12. Tian W., Liu X., and Yu W. - Research progress of gas sensor based on graphene and its derivatives: A review, *Appl. Sci.* **8** (2018) 1118.

13. Zhang J., Liu X., Neri G., and Pinna N. - Nanostructured materials for room-temperature gas sensors, *Adv. Mater.* **28** (2016) 795-831.
14. Le X. V., Luu T. L. A., Nguyen H. L., and Nguyen C. T. - Synergistic enhancement of ammonia gas-sensing properties at low temperature by compositing carbon nanotubes with tungsten oxide nanobricks, *Vacuum* **168** (2019) 108861.
15. Korotcenkov G., Brinzari V., Ivanov M., Cerneavski A., Rodriguez J., and Cirera A. - Structural stability of indium oxide films deposited by spray pyrolysis during thermal annealing, *Thin Solid Films* **479** (2005) 38-51.
16. Righettoni M., Amann A., and Pratsinis S. E. - Breath analysis by nanostructured metal oxides as chemo-resistive gas sensors, *Mater. Today* **18** (2015) 163-171.
17. Nguyen V. D., Nguyen D. H., Nguyen T. D., Dang T. T. L., and Nguyen V. H. - Ammonia-gas-sensing characteristics of WO₃/Carbon nanotubes nanocomposites: Effect of nanotube content and sensing mechanism, *Sci. Adv. Mater.* **8** (2016) 524-533.
18. Le X. V., Duong V. T., Luu T. L. A., , Pham V. T., and Nguyen H. L. - Composition of CNT and WO₃ nanoplate: Synthesis and NH₃ gas sensing characteristics at low temperature, *J. Met. Mater. Miner.* **29** (2019) 61-68.
19. Zheng H., Ou J. Z., Strano M. S., Kaner R. B., Mitchell A., and Kalantar-Zadeh K. - Nanostructured tungsten oxide - Properties, synthesis, and applications, *Adv. Funct. Mater.* **21** (2011) 2175-2196.
20. Dong P., Hou G., Xi X., Shao R., and Dong F. - WO₃-based photocatalysts: morphology control, activity enhancement and multifunctional applications, *Environ. Sci. Nano* **4** (2017) 539-557.
21. Chu M. H., Do Q. D., Nguyen V. D., Vu V. Q., Nguyen V. Toan, Nguyen V. H., Nguyen D. H. - Facile synthesis of ultrafine rGO/WO₃ nanowire nanocomposites for highly sensitive toxic NH₃ gas sensors, *Mater. Res. Bull.* **125** 110810.
22. Salama T. M., Morsy M., Shahba R. M. A., Mohamed S. H., and Mohamed M. M. - Synthesis of graphene oxide interspersed in hexagonal WO₃ nanorods for high-efficiency visible-light driven photocatalysis and NH₃ gas sensing, *Front. Chem.* **7** (2019) 1-14.
23. Jeevitha G., Abhinayaa R., Mangalaraj D., Ponpandian N., Meena P., Mounasamy V., Madanagurusamy S. - Porous reduced graphene oxide (rGO)/WO₃ nanocomposites for the enhanced detection of NH₃ at room temperature, *Nanoscale Adv.* **1** (2019) 1799-1811.
24. Paulchamy B., Arthi G., and Lignesh BD - A simple approach to stepwise synthesis of graphene oxide nanomaterial, *Nanomedicine Nanotechnol.* **6** (2015) 1000253.
25. Luu T. L. A., Pham T. P., Han V. P., Duong V. T., Le X. V., Pham T. S., Do D. T., Dang D. V., Nguyen H. L., Nguyen C. T., - Tailoring the tructure and morphology of WO₃ nanostructures by hydrothermal method, *Vietnam J. Sci. Technol.* **56** (2018) 127-134.
26. Hosseini F., Rasuli R., and Jafarian V. - Immobilized WO₃ nano-particles on graphene oxide as a photo-induced antibacterial agent against UV resistant *Bacillus Pumilus*, *J. Phys. D. Appl. Phys.* **51** (2018) 145403.
27. Hu X., Xu P., Gong H., and Yin G. - Synthesis and characterization of WO₃/graphene nanocomposites for enhanced photocatalytic activities by one-step in-situ hydrothermal reaction, *Materials (Basel).* **11** (2018) 147.
28. Flores-Mena J. E., Diaz-Reyes J., and Balderas-Lopez J. A. - Structural properties of WO₃

- dependent of the annealing temperature deposited by hot-filament metal oxide deposition Rev. Mex. Fis. **58** (2012) 504-509.
29. Daniel M. F., Desbat B., Lassegues J. C., Gerand B., and Figlarz M. - Infrared and Raman study of WO_3 tungsten trioxides and $WO_3 \cdot xH_2O$ tungsten trioxide hydrates, J. Solid State Chem. **67** (1987) 235-247.
 30. Dresselhaus M. S., Jorio A., and Saito R. - Characterizing graphene, graphite, and carbon nanotubes by Raman spectroscopy, Annu. Rev. Condens. Matter Phys. **1** (2010) 89-108.
 31. Jeevitha G., Abhinayaa R., Mangalaraj D., and Ponpandian N. - Tungsten oxide-graphene oxide (WO_3 -GO) nanocomposite as an efficient photocatalyst, antibacterial and anticancer agent, J. Phys. Chem. Solids **116** (2018) 137-147.
 32. Fu L., Xia T., Zheng Y., Yang J., Wang A., and Wang Z. - Preparation of WO_3 -reduced graphene oxide nanocomposites with enhanced photocatalytic property, Ceram. Int. **41** (2015) 5903-5908.
 33. Tahir M. B., Nabi G., and Khalid N. R. - Enhanced photocatalytic performance of visible-light active graphene- WO_3 nanostructures for hydrogen production, Mater. Sci. Semicond. Process. **84** (2018) 36-41.
 34. Ojha K., Anjaneyulu O., and Ganguli A. K. - Graphene-based hybrid materials : synthetic approaches and properties, Curr. Sci. **107** (2018) 397-418.
 35. Moseley P. T. - Progress in the development of semiconducting metal oxide gas sensors: a review, Meas. Sci. Technol. **28** (2017) 82001.
 36. Wei Y., Hu M., Wang D., Zhang W., and Qin Y. - Room temperature NO_2 - sensing properties of porous silicon/tungsten oxide nanorods composite, J. Alloys Compd. **640** (2015) 517-524.
 37. Alshammari A. S., Alenezi M. R., Lai K. T., and Silva S. R. P. - Inkjet printing of polymer functionalized CNT gas sensor with enhanced sensing properties, Mater. Lett. **189** (2017) 299-302.

Supplement document

Table S1. Components of nanocomposite and WO₃ suspensions prepared for sensors fabrication.

Sample	100-ppm GO suspension		Water (ml)	WO ₃ powder (g)	Nanocomposite (WO ₃ +GO) suspension	
	Volume (ml)	GO content (g)			Volume (ml)	Nanocomposite (WO ₃ +GO) content (g)
0.1%GO @WO ₃	1	0.0001	4	0.0999	5	0.1000
0.3%GO @WO ₃	3	0.0003	2	0.0997	5	0.1000
0.5%GO @WO ₃	5	0.0005	0	0.0995	5	0.1000
WO ₃	0	0	5	0.1000	5	0.1000

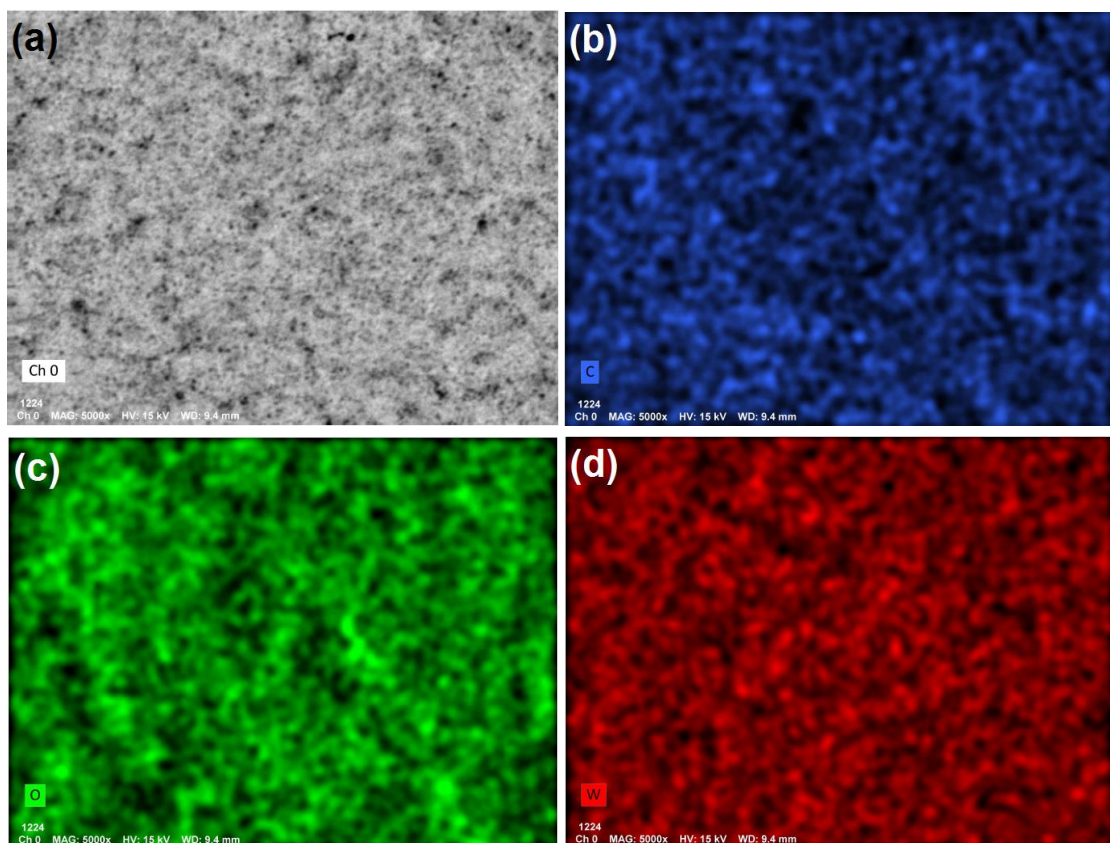


Figure S1. Low magnification SEM image (x5000) (a), and mapping EDS images of 0.5%GO@WO₃ sample: (b) the distribution of C, (c) the distribution of O element, and (d) the distribution of W element.

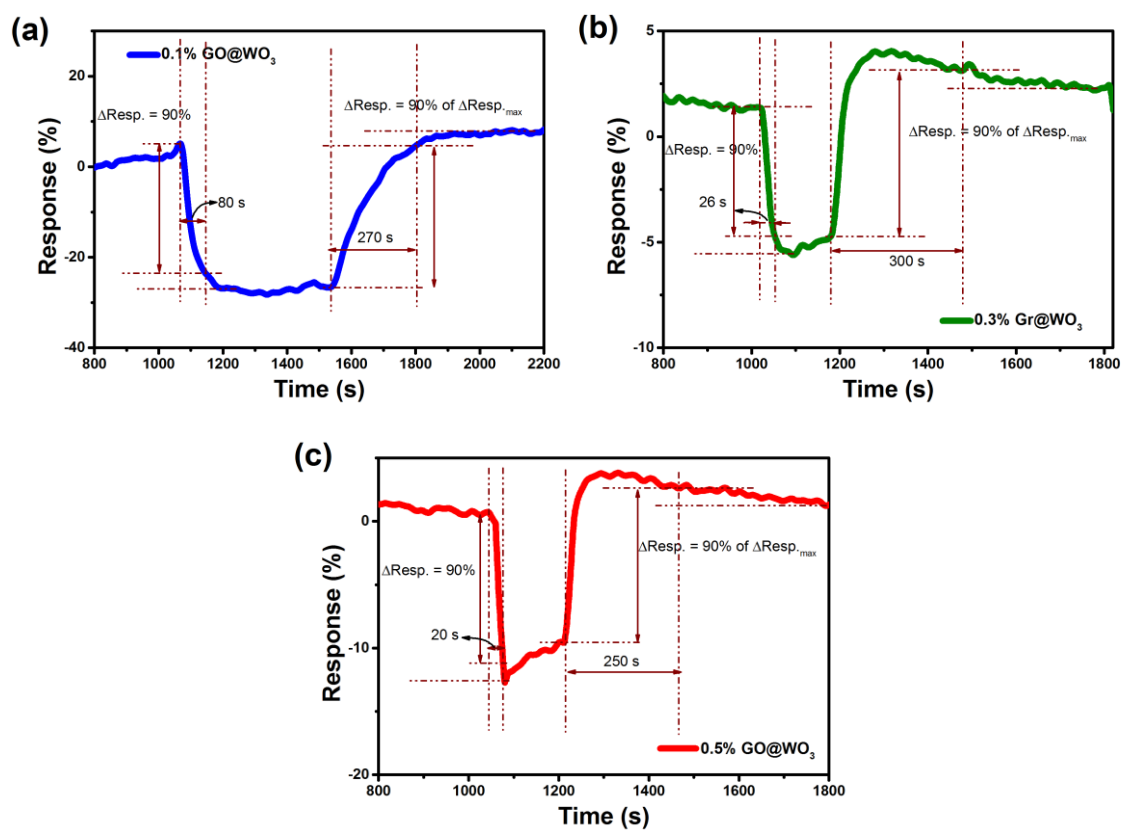


Figure S2. Response and recovery times determination from response revolution of samples: (a) 0.1 %GO@WO₃, (b) 0.3 %GO@WO₃ and (c) 0.5 %GO@WO₃.